Multicarrier Signal Unfolding for 25% Capacity Improvement in Optical Fiber Transmission

Yinglin Chen*, Tianhua Xu$, and Tongyang Xu†

*6G Research Center, China Telecom Research Institute, Guangzhou 510660, China
$School of Engineering, University of Warwick, Coventry CV4 7AL, United Kingdom
†Department of Electronic and Electrical Engineering, University College London, London WC1E 7JE, United Kingdom
Email: chenyl37@chinatelecom.cn, tianhua.xu@warwick.ac.uk, tongyang.xu.11@ucl.ac.uk

***Abstract*—Spectrally efficient frequency division multiplexing (SEFDM) can achieve improved spectral efficiency than orthogonal frequency division multiplexing (OFDM) waveform by narrowing subcarrier spacing. However, the resulting inter-carrier interference (ICI) limits the performance of simple detectors such as matched filter (MF). Traditional iterative detection (ID) has competitive detection performance via cancelling interference iteratively and comparing symbols with manually defined thresholds. Unfolding the ID detector results in a stacked architecture similar to a multi-layer neural network (NN). This architecture allows the combination of NN and the ID process in each iteration, where the ID process is mathematically deterministic. This work proposes an unfolding detector which adjusts an available symbol threshold mapping result via NN processing, potentially giving us the optimal threshold mapping scheme. Simulation results show that the proposed unfolding detector achieves better error performance on SEFDM signal detection than traditional detectors, across all examined optical fiber transmission distances. Furthermore, it exhibits close error performance to OFDM with a 25% spectral efficiency gain.**

***Index Terms*—Unfolding, optical fiber communication, neural network, interference cancellation, iterative detection, SEFDM.**

I. Introduction

Moving into the 6G era, operators are increasingly driven to optimize optical systems to support higher throughput. Orthogonal frequency division multiplexing (OFDM) waveform has been broadly adopted in optical transmission systems [1]. While OFDM subcarriers are orthogonally spaced by the symbol rate to avoid inter-carrier interference (ICI), spectrally efficient frequency division multiplexing (SEFDM) was introduced with relaxed orthogonality constraints, allowing for flexible waveform design and improved spectral efficiency [2].

The basic principle of the SEFDM waveform is to achieve higher spectral efficiency via compressing subcarrier spacing. One challenge introduced by the waveform is ICI. To recover signals from such interference, many solutions have been proposed and tested. Maximum likelihood (ML) provides optimal performance at the cost of impractically high computational burden. Simple detection methods matched filter (MF) and zero forcing (ZF) have worse bit-error-rate (BER) performance. The traditional iterative detection technique is successive interference cancellation (SIC), which cancels interference iteratively. A more advanced iterative solution is termed iterative detection (ID) [3], [4], which can jointly use SIC and a linear threshold mapping scheme to get higher accuracy. Recently, the advancement of artificial intelligence (AI) enables neural networks (NN) assisted signal detection. Single-layer neural networks were first applied for basic detection tasks. Later, multiple layers were stacked leading to deep learning (DL) neural networks [5]. DL has been applied to recover OFDM signals in [6]. Previous work in [7] has evaluated the capability of using DL to recover SEFDM signals but with limited performance gain.

This work investigates the integration of DL neural networks with traditional ID method, for SEFDM signal detection in long-haul optical fiber transmission. The iterative nature of ID lends itself to the use of deep unfolding. The initial work on deep unfolding was introduced in sparse coding [8], which aims at simplifying each iteration of the iterative shrinkage and thresholding (ISTA) algorithm through neural network layers. It was also successfully adopted in OFDM signal detection [9], where iterative orthogonal approximate message passing algorithm was unfolded with its two parameters adjusted by DL. When combined with ID in this work, deep unfolding learns the thresholds involved in interference cancellation and fine tunes output results at each iteration. Subsequent iterations will then have more accurate input estimates and therefore output a better estimation. The proposed unfolding detector is evaluated using 4QAM and 16QAM in additive white Gaussian noise (AWGN) channel and is further validated in optical environments. The unfolding detector reduces the required launch power compared to traditional detectors. Furthermore, it enables SEFDM to exhibit BER performance comparable to OFDM while offering higher spectral efficiency.

II. System Model

This section describes a long-haul optical system that utilizes SEFDM signals for improved spectral efficiency.

A. SEFDM Fundamentals

SEFDM enhances spectral efficiency by reducing the spacing between subcarriers, placing them closer together than

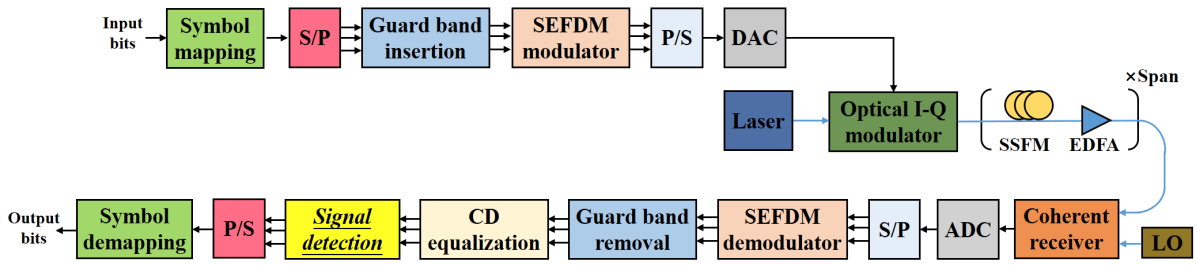

Fig. 1. Block diagram of the optical fiber communication system with the detection designed for ICI-impaired SEFDM signals. S/P: serial to parallel; P/S: parallel to serial; DAC: digital-to-analog converter; ADC: analogue-to-digital converter; SSFM: split-step Fourier method; EDFA: erbium-doped fiber amplifier; Optical I-Q modulator: optical in-phase and quadrature modulator; LO: local oscillator; CD equalization: chromatic dispersion equalization.

the orthogonal spacing used in traditional OFDM systems. An SEFDM signal is given by:

$$X_k = \frac{1}{\sqrt{Q}} \sum_{n=0}^{N-1} s_n \exp\left(\frac{j2\pi nk\alpha}{Q}\right), \tag{1}$$

with the parameters defined as follows: X_k denotes the time-domain sample at index k, where $k = 0, 1, ..., Q-1$. The number of time-domain samples is given by $Q = \rho N$, where N is the number of subcarriers and ρ is the oversampling factor. A normalization factor of $\frac{1}{\sqrt{Q}}$ is applied to maintain unit average power. The term s_n corresponds to the n^{th} single-carrier symbol within one SEFDM symbol. Finally, the bandwidth compression factor is defined as $\alpha = \Delta f \cdot T$, where Δf is the subcarrier spacing and T is the symbol duration.

The SEFDM signal in (1) can be represented in matrix form as:

$$X = \mathbf{F}S, \tag{2}$$

where $\mathbf{F}$ denotes the subcarrier matrix. When the signal is transmitted through a noisy channel, the received signal turns into:

$$Y = \mathbf{F}S + Z, \tag{3}$$

with Z representing AWGN terms. Signal recovery is performed by multiplying the received signal with the conjugate transpose of the subcarrier matrix, $\mathbf{F}^*$, resulting in:

$$R = \mathbf{F}^*\mathbf{F}S + \mathbf{F}^*Z = \mathbf{C}S + W, \tag{4}$$

where $\mathbf{C} = \mathbf{F}^*\mathbf{F}$ is the $N \times N$ correlation matrix, and W is the resulting demodulated noise vector. Specifically, the non-zero off-diagonal elements in $\mathbf{C}$ characterise the ICI due to non-orthogonal subcarriers, formulated as

$$\mathbf{C}_{g,n} = \begin{cases} 1 & , g = n \\ \frac{1}{Q}\frac{1-\exp[j2\pi\alpha(g-n)]}{1-\exp[j2\pi\alpha(g-n)/Q]} & , g \neq n \end{cases}. \tag{5}$$

B. Fiber Transmission Scheme

The SEFDM signals are transmitted in a long-haul optical fiber system, as illustrated in Fig. 1. Input bits are mapped to a serial of single-carrier data symbols, which are then converted to parallel streams for multi-carrier modulation. Oversampling is performed by adding guard bands at both sides of the signal spectrum. Following SEFDM modulation, as defined in (2), and parallel-to-serial conversion, the SEFDM symbols are generated. These symbols are subsequently converted into analog form and modulated onto an optical carrier with a 320 GHz bandwidth, centered at a laser wavelength of 1550 nm.

Long-haul optical fiber transmission is modeled by connecting multiple 80 km spans in series. To include Kerr fiber non-linear effects, the optical fiber channel in each span is simulated by solving the nonlinear Schrödinger equation using the split-step Fourier method (SSFM) with a step size of 0.05 km [10]. In this work, the non-linear coefficient is specified as 1.2 W·km, and the chromatic dispersion (CD) parameter is set to 17 ps/(nm·km). Considering an attenuation constant of 0.2 dB/km, an erbium-doped fiber amplifier (EDFA) is applied at the end of each span to compensate for power loss. The EDFA noise figure is 4.5 dB.

At the receiving side, the optical signals are mixed with an ideal local oscillator (LO) laser in the coherent receiver. The output electrical signals are then digitized in the analogue-to-digital conversion (ADC) module. After converting to parallel SEFDM symbol streams, SEFDM demodulation is carried out using (4), followed by the removal of guard bands. Since fiber dispersion is a linear effect, CD will be perfectly mitigated via existing frequency-domain equalization techniques [11]. In the signal detection stage, the compensated and demodulated signals are processed by a detector robust to self-created ICI within SEFDM, which will be proposed in the next section. Then, the estimated data symbols are converted back to serial form and demapped to yield the final output bits.

III. Detection Designs

This section proposes an unfolding detector design inspired by tradition ID detector and neural networks.

A. Traditional Iterative Detection

The traditional ID approach is shown in Fig. 2, which consists of an interference cancellation (IC) block and a threshold mapping block. The IC block operates by

$$s_i^{l+1} = \varphi(R_i^{l+1} - \sum_j \mathbf{\Psi}_{ij}^{l+1} s_j^l), \tag{6}$$

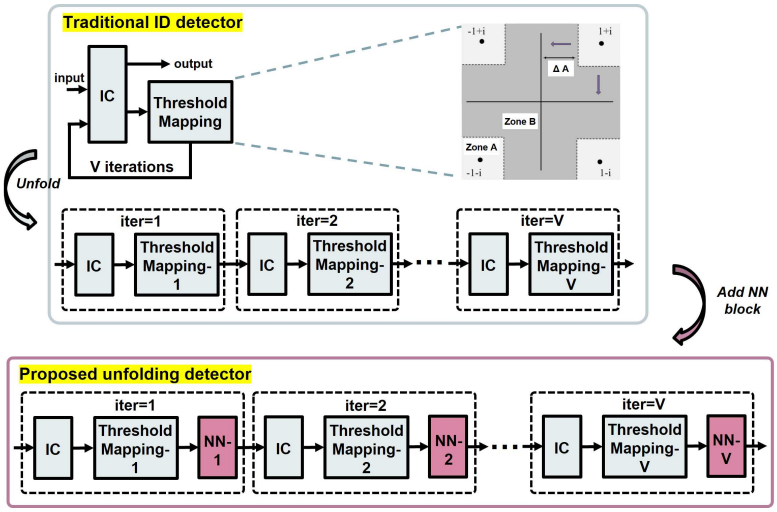

Fig. 2. Block diagram of traditional ID detector and proposed unfolding detector.

where s_i^{l+1} denotes the i^{th} element at $(l+1)^{th}$ iteration, and s_j^l denotes the j^{th} element at l^{th} iteration. $\varphi(\cdot)$ is a mapping function determined by the threshold mapping block. R_i^{l+1} and $\mathbf{\Psi}_{ij}^{l+1}$ indicate the i^{th} demodulated symbol and the correlation-ICI element at $(l+1)^{th}$ iteration, respectively. The correlation-ICI matrix $\mathbf{\Psi}$ is defined by removing the diagonal elements in (5):

$$\mathbf{\Psi} = \mathbf{C} - \mathbf{I}, \tag{7}$$

where $\mathbf{I}$ is an $N \times N$ identity matrix. Since R and $\mathbf{\Psi}$ do not change in each iteration, the expression in (6) can be simplified into

$$s_i^{l+1} = \varphi(R_i - \sum_j \mathbf{\Psi}_{ij} s_j^l). \tag{8}$$

To facilitate efficient information exchange between iterations, $\varphi(\cdot)$ utilizes an adaptive decision threshold, which adjusts after each iteration. In Fig. 2, 4QAM is provided as an example. Two regions are defined in the decision process: Zone A and Zone B. Meanwhile, an uncertainty interval is defined as ΔA. Symbols that lie outside the uncertainty interval ΔA (i.e. within Zone A) are hard decided to their nearest 4QAM constellation points. In contrast, symbols within Zone B remain unchanged and are carried over to the next iteration. As interference cancellation progresses and symbol estimates improve, the uncertainty interval ΔA decreases with each iteration. This iterative narrowing continues until all symbols converge to 4QAM hard-decision symbols in the last iteration.

According to [3], the uncertainty interval ΔA can iterate with linear reduction, defined as $\Delta A = 1 - m/V$, where V is the total number of iterations and m is the m^{th} iteration. When $m = V$, $\Delta A = 0$ indicating the transition to traditional 4QAM hard-decision detection. Algorithm 1 describes this process. However, such analytically determined threshold strategy may not be optimal. This provides ground for exploring DL-assisted approaches to derive optimal thresholds.

Algorithm 1 : Traditional ID detector for 4QAM.

Input: $R, \mathbf{C}, S, V$;
Output: $\bar{S}$;
for $m = 1$; $m \leq V$; $m++$ **do**
  $\hat{S} = R - (\mathbf{C} - \mathbf{I})S$; $\Rightarrow$ {Interference cancellation}
  $S = \varphi(\hat{S})$; $\Rightarrow$ {Threshold mapping function}
  $d = 1 - \frac{m}{V}$; $\Rightarrow$ {Uncertainty interval}
  $\hat{S}_{\Re} = Real(\hat{S})$;
  $\hat{S}_{\Im} = Imag(\hat{S})$;
  if $\hat{S}_{\Re} > d \& \hat{S}_{\Im} > d$ **then**
    $S = 1 + i$;
  else if $\hat{S}_{\Re} > d \& \hat{S}_{\Im} < -d$ **then**
    $S = 1 - i$;
  else if $\hat{S}_{\Re} < -d \& \hat{S}_{\Im} > d$ **then**
    $S = -1 + i$;
  else if $\hat{S}_{\Re} < -d \& \hat{S}_{\Im} < -d$ **then**
    $S = -1 - i$;
  else
    $S = \hat{S}$;
  end if } Threshold mapping
end for
$\bar{S} = S$;

B. Proposed Unfolding Detection

DL with neural networks can automatically extract complex hidden features from the signal, with these features being used to assist in symbol detection. A neural network is composed of multiple layers, where the connections between neurons in each layer can be described by the following expression:

$$x_i^{k+1} = \sigma(\sum_j \mathbf{W}_{ij}^{k+1} x_j^k + b_i^{k+1}). \tag{9}$$

Here, x_i^{k+1} denotes the i^{th} element in the $(k+1)^{th}$ layer, and x_j^k represents the j^{th} element in the k^{th} layer. $\mathbf{W}_{ij}^{k+1}$

Table I: Training configuration parameters.

Parameter	Value
Training / Validation symbols	4000 / 1000
Epochs	40
Mini-batch size	16
Initial learning rate	0.02
Learning rate reduction	Factor 0.2 after 20 epochs
Dropout rate	50%
L_2 regularization factor	0.0001
Optimizer	SGDM (momentum=0.9)
Activation function	ReLU
Data shuffling	Each epoch

is the weight element in the $(k+1)^{th}$ layer, and b_i^{k+1} is the i^{th} bias in the $(k+1)^{th}$ layer. The weights and biases are adjustable and are updated through backpropagation using optimization algorithms. The function $\sigma(\cdot)$ represents the activation function. Rectified linear units (ReLU) is typically used as the default activation function, which is given as

$$ReLU(x) = max\{x, 0\}. \tag{10}$$

The mathematical formulations for ID in (8) and for neural networks in (9) can be reformulated in matrix form, as shown in (11) and (12), respectively:

$$S^{\lambda} = \varphi(-\mathbf{\Psi} S^{\lambda-1} + R), \tag{11}$$

$$X^{\lambda} = \sigma(\mathbf{W} X^{\lambda-1} + B), \tag{12}$$

where λ is the λ^{th} iteration in (11) and the λ^{th} layer in (12).

The ID algorithm in (11) shares a similar structure with the multi-layer neural network described in (12). As illustrated by Fig. 2, the ID detector, after unfolding operation, results in a layered architecture that closely resembles a multi-layer neural network. Given that analytically derived thresholds may not be optimal, we propose to enhance the ID detector by incorporating NN layers at the end of each ID iteration (i.e. ID layer). The architecture of the resulting unfolding detector is presented in Fig. 2. Each NN block within an ID layer operates independently. As interference cancellation becomes increasingly accurate with each iteration, the learnt weights and biases within the corresponding NN blocks are adjusted independently to optimize threshold mapping and enhance overall performance. The unfolding detector can be mathematically expressed as

$$\begin{aligned} X^2 &= \sigma(\mathbf{W}\varphi(-\mathbf{\Psi}S^1 + R)^1 + B), \\ X^3 &= \sigma(\mathbf{W}\varphi(-\mathbf{\Psi}X^2 + R)^2 + B), \\ &\vdots \\ X^V &= \sigma(\mathbf{W}\varphi(-\mathbf{\Psi}X^{V-1} + R)^{V-1} + B). \end{aligned} \tag{13}$$

IV. Results and Discussions

This section provides the BER performance and complexity analysis of the unfolding detector.

Table II: Architecture and dimension for unfolding detector.

Unfolding detector	
Layer	Dimension
IC	1×1×16
Reshape	1×1×32
Threshold Mapping	1×1×32
IC1-FullConnection1	1×1×64
IC1-BatchNorm	1×1×64
IC1-ReLU	1×1×64
IC1-FullConnection2	1×1×32
Reshape	1×1×16
IC	1×1×16
Reshape	1×1×32
Threshold Mapping	1×1×32
IC2-FullConnection1	1×1×64
IC2-BatchNorm	1×1×64
IC2-ReLU	1×1×64
IC2-FullConnection2	1×1×32
Reshape	1×1×16
.	.
.	.
.	.
IC	1×1×16
Reshape	1×1×32
Threshold Mapping	1×1×32
IC10-FullConnection1	1×1×64
IC10-BatchNorm	1×1×64
IC10-ReLU	1×1×64
IC10-FullConnection2	1×1×32

A. Training Configurations

We generate 5000 random SEFDM symbols, all configured with $\alpha = 0.8$ and $N = 16$. Parameters for training are listed in Table I. The ID detector operates with $V = 10$ iterations and linear reduction for threshold mapping reused from previous work [3]. For a fair comparison, the unfolding detector also has 10 cascaded ID layers, and its architecture is listed in Table II [1]. This work considers SEFDM signals with 4QAM and 16QAM modulation. Given that SEFDM signals comprise 16 subcarriers, the input dimension of NN processing is 32—consisting of 16 real and 16 imaginary components. Each NN block includes two fully connected hidden layers: the first with 64 neurons and the second with 32 neurons. Batch normalization and ReLU activation functions are inserted between consecutive fully connected layers.

B. Error Performance Comparisons

We first present the detection performances obtained in AWGN channel, and then test the best performing detectors in optical fiber channel. In Fig. 3, the iterative-based ID detector, which iteratively removes ICI and improves detection accuracy, outperforms simple MF and ZF detectors. The proposed unfolding detector, enhanced by NN blocks fine tuning the output of each iteration, exhibits better detection performance than ID detector. In addition, the performance of OFDM signals modulated with 4QAM is provided. Since OFDM does not involve bandwidth compression and consequently experiences no ICI, the use of ID or unfolding detectors

[1]We tested different architectures for NN blocks, and the chosen configuration provided satisfactory performance with acceptable complexity.

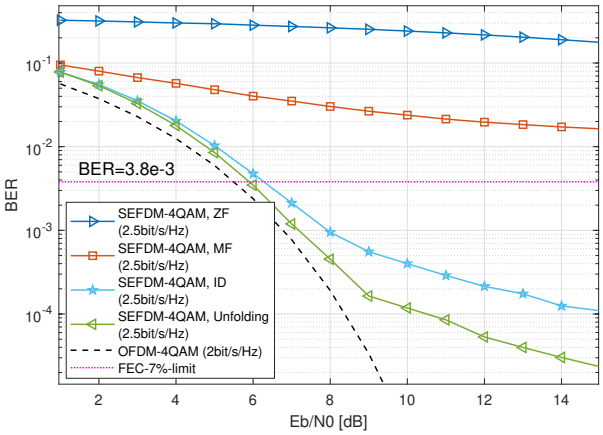

Fig. 3. BER performances for 4QAM-modulated SEFDM signals with traditional detectors and the proposed unfolding detector, when transmitted in AWGN channel.

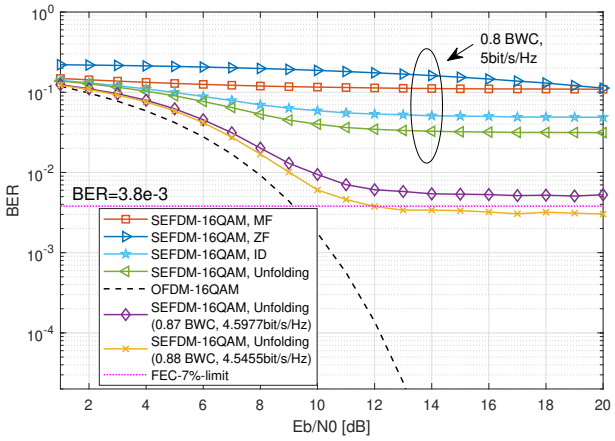

Fig. 4. BER performances for 16QAM-modulated SEFDM signals with traditional detectors and the proposed unfolding detector, when transmitted in AWGN channel. BWC indicates bandwidth compression factor α, whose default value is 0.8 unless otherwise specified.

cannot improve BER performance for these signals. Therefore, OFDM signals are operated with MF detector. Compared to OFDM signals, SEFDM signals using the unfolding detector achieve a spectral efficiency gain of 0.5 bit/s/Hz, while requiring only an additional 0.4 dB of transmission power to reach the 7% forward error correction (FEC) limit, corresponding to a BER of 3.8×10^{-3}.

In Fig. 4, SEFDM and OFDM signals are modulated with 16QAM. When operated with the default bandwidth compression level at $\alpha = 0.8$, the spectral efficiency value of SEFDM signals increase to 5 bit/s/Hz. While the unfolding detector still exhibits the best detection performance over other existing detectors, it fails to reach FEC limit, as the residual ICI after interference cancellation and NN tuning remain high to affect symbol detection. By increasing the bandwidth compression factor to $\alpha = 0.88$, SEFDM with the unfolding detector reaches FEC limit with 3 dB power penalty compared to OFDM. The advantage of SEFDM over OFDM is more noticeable under low modulation cardinality and therefore only 4QAM is considered for the rest simulations.

Performance comparisons between the proposed unfolding detector and two traditional detectors are presented for a fiber transmission distance of 8000 km (100 spans) in Fig. 5. The simple MF detector lacks interference cancellation capabilities and is therefore ineffective for SEFDM signals, similar to its performance in the AWGN scenario. We observe that the unfolding detector obtains 1.2 dB performance gain over the ID detector when crossing FEC limit. Meanwhile, it enables SEFDM signals to achieve a spectral effciency gain of 0.5 bit/s/Hz while requiring slightly higher launch power, compared to OFDM signals.

Detection performances in terms of the launch power required to reach the FEC limit at different transmission distances are provided in Fig. 6. Due to fiber non-linearities which increase with fiber length, the required launch power

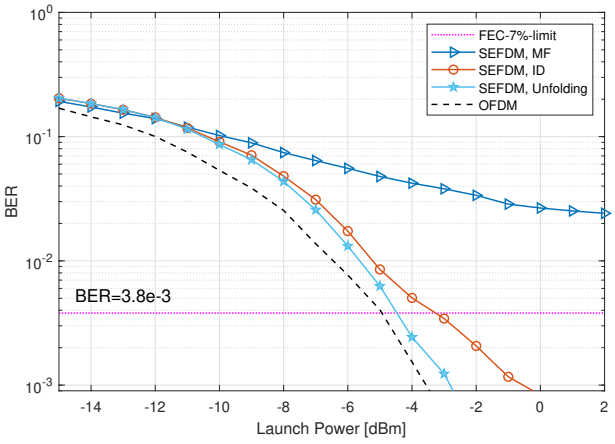

Fig. 5. BER performances for the unfolding detector transmitted over 8000 km optical fiber, compared with traditional MF and ID detectors.

for all detectors increases as the fiber length increases, while they still maintain successful data transmission under FEC. Over 2400 km to 12000 km fiber transmission, the proposed unfolding detector consistently exhibits higher accuracy than the ID detector, and hence requires lower launch power. Moreover, the power penalty of SEFDM with the unfolding detector at 2.5 bit/s/Hz compared to OFDM at 2 bit/s/Hz remains small across all investigated transmission distances.

C. Complexity Analysis

According to the architecture shown in Fig. 2, the computational complexity of the proposed unfolding detector arises from IC operations, threshold mapping, and NN processing.

For IC operations given by (11), there is a multiplication between a square matrix and a vector, followed by an addition between two vectors. The number of real values is

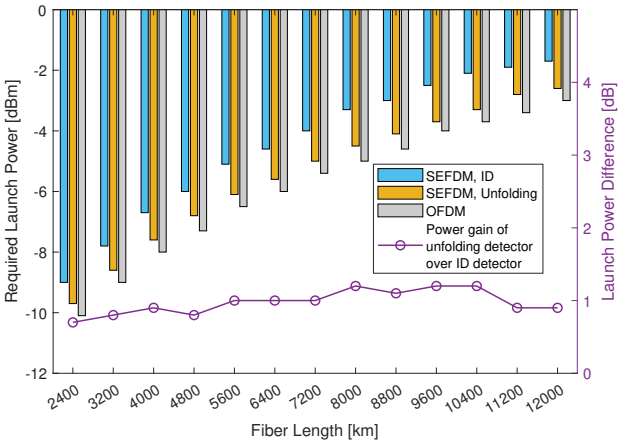

Fig. 6. Required launch power to achieve the 7% FEC limit across fiber transmission distances from 2400 km to 12000 km. Launch power gain of the unfolding detector over ID detector is consistently around 1 dB, as shown in purple line.

$2N$ per SEFDM symbol, and therefore the computational complexity for one IC operation is $(2N)^2$ multiplications and $2N$ additions. Then, threshold mapping involves only a comparison for decision-making. Therefore, it is not taken into account in computational complexity. NN processing includes the computation of weight, bias, normalization mean, and normalization variance. Based on the dimension in Table II, there are $(4N)^2$ multiplications and $4N$ additions for the first fully connected layer, and $(2N)^2$ multiplications and $2N$ additions for the second fully connected layer. The reshape operation is not considered in the computational complexity. ReLU is essentially a selector and therefore it is excluded from the computational complexity analysis. To simplify expressions, we use ϵ and υ to notate the number of multiplications and the number of additions in each batch normalization layer, respectively. The computational complexity of the unfolding detector is the sum of the previous operations times the number of layers V, as shown in Table III.

Since ID detector has no NN processing, its complexity only includes IC operations and threshold mapping. Table III shows that the performance gain achieved unfolding detector has higher computational complexity. However, the unfolding detection architecture suggests that the combination of DL algorithms and iteration detection is feasible and more importantly, it can achieve improved detection accuracy.

V. Conclusion

This work proposed an interpretable and intelligent signal detector for SEFDM signals. Since SEFDM subcarriers are spaced closer than the orthogonal limit, ICI effects need to be considered in SEFDM signal detection. The traditional iterative detector (ID) cancels interference iteratively and performs adaptive threshold mapping. However, the manually defined threshold mapping scheme may not be optimal. This motivated us to utilize advanced DL algorithms capable of automatic feature extraction. By unfolding the iterative operation, the ID detector becomes a stack of ID layers, resembling a multi-layer neural network (NN). Then an NN block is added at the end of each ID block to fine tune the mapping results. The proposed unfolding detector were tested with 4QAM and 16QAM modulation in AWGN and various long-haul fiber environments. BER results show that the unfolding detector consistently outperforms traditional ID detector. Moreover, SEFDM signals using the unfolding detector achieve BER performance comparable to OFDM, while offering a 25% increase in spectral efficiency.

Table III: Computational complexity comparison in terms of real-value multiplications and real-value additions. ϵ and υ are the number of real-value multiplications and the number of real-value additions at each batch normalization layer, respectively. N is the number of subcarriers. V is the number of ID layers, same as the number of iterations for ID detector.

Detector	Multiplication	Addition
ID detector	$V\left(4N^2\right)$	$V\left(2N\right)$
Unfolding detector	$V\left(24N^2+\epsilon\right)$	$V\left(8N+\upsilon\right)$

VI. Acknowledgement

This work was supported in part by the UK Engineering and Physical Sciences Research Council (EPSRC) under Grant EP/Y000315/2, and in part by EU Horizon 2020 Grant 101008280 (DIOR), UK Royal Society Grant (IES/R3/223068), EU Horizon Europe Grant 101236637 (SPAR), EU Horizon Europe Grant 101131146 (UPGRADE).

References

[1] J. Armstrong, "OFDM for optical communications," *J. Lightw. Technol.*, vol. 27, no. 3, pp. 189–204, 2009.

[2] T. Xu and I. Darwazeh, "Transmission experiment of bandwidth compressed carrier aggregation in a realistic fading channel," *IEEE Transactions on Vehicular Technology*, vol. 66, no. 5, pp. 4087–4097, May 2017.

[3] T. Xu, R. C. Grammenos, F. Marvasti, and I. Darwazeh, "An improved fixed sphere decoder employing soft decision for the detection of non-orthogonal signals," *IEEE Commun. Lett.*, vol. 17, no. 10, pp. 1964–1967, Oct. 2013.

[4] Z. Hu and C.-K. Chan, "A novel baseband faster-than-Nyquist non-orthogonal FDM IM/DD system with block segmented soft-decision decoder," *J. Lightw. Technol.*, vol. 38, no. 3, pp. 632–641, 2020.

[5] C. Zhang, P. Patras, and H. Haddadi, "Deep learning in mobile and wireless networking: A survey," *IEEE Commun. Surveys Tuts.*, vol. 21, no. 3, pp. 2224–2287, 2019.

[6] H. Ye, G. Y. Li, and B. H. Juang, "Power of deep learning for channel estimation and signal detection in OFDM systems," *IEEE Wireless Commun. Lett.*, vol. 7, no. 1, pp. 114–117, Feb. 2018.

[7] T. Xu, T. Xu, and I. Darwazeh, "Deep learning for interference cancellation in non-orthogonal signal based optical communication systems," in *2018 Progress in Electromagnetics Research Symposium - Spring (PIERS)*, Aug. 2018 (invited), pp. 241–248.

[8] K. Gregor and Y. LeCun, "Learning fast approximations of sparse coding." Omnipress, 2010.

[9] J. Zhang, H. He, C. Wen, S. Jin, and G. Y. Li, "Deep learning based on orthogonal approximate message passing for CP-free OFDM," in *ICASSP 2019 - 2019 IEEE International Conference on Acoustics, Speech and Signal Processing (ICASSP)*, 2019, pp. 8414–8418.

[10] G. Agrawal, *Nonlinear Fiber Optics (Fifth Edition)*, 5th ed. Academic Press, 2013.

[11] S. J. Savory, "Digital filters for coherent optical receivers," *Opt. Express*, vol. 16, no. 2, pp. 804–817, Jan 2008.